Title	Comparison of quadratic and power law for nonlinear flow through porous media
Author(s)	Cheng, Nian-Sheng; Hao, Zhiyong; Tan, Soon Keat
Citation	Cheng, N. S., Hao, Z., & Tan, S. K. (2008). Comparison of quadratic and power law for nonlinear flow through porous media. Experimental Thermal Fluid Science, 32(8), 1538-1547.
Date	2008
URL	http://hdl.handle.net/10220/7670
Rights	© 2008 Elsevier. This is the author created version of a work that has been peer reviewed and accepted for publication by Experimental thermal fluid science, Elsevier. It incorporates referee's comments but changes resulting from the publishing process, such as copyediting, structural formatting, may not be reflected in this document. The published version is available at: [DOI: http://dx.doi.org/10.1016/j.expthermflusci.2008.04.007].

Comparison of Quadratic and Power Law for Nonlinear Flow through Porous Media

Nian-Sheng Cheng, Zhiyong Hao, and Soon Keat Tan

School of Civil and Environmental Engineering
Nanyang Technological University, Singapore 639798
Tel: 65-6790 6936; Fax: 65-6791 0676; Email: cnscheng@ntu.edu.sg

---

Abstract: The quadratic and power laws are two typical formulations that can be used to extend the Darcy law to non-Darcy flows through porous media. Both laws are reformulated in the dimensionless form in this study. They are then evaluated by fitting to experimental data with specified variations in seepage velocity, which were specifically collected for a simplified ordered porous model. The results show that the quadratic law is applicable to both linear and nonlinear flow regimes but the two coefficients vary at different regimes. In comparison, the power law appears not workable if the seepage velocity varies over a wide range. This study also demonstrates that the two parameters included in the power law are generally interrelated, and the relationship derived based on the quadratic law compares well with the experimental results. To help understand the non-linear behavior associated with the simplified porous model, CFD simulations were also performed to visualize and elucidate localized 3D flow phenomena.

Keywords: Porous media; Darcy law; Inertial effect; Turbulence; Nonlinear flow; Seepage; Power law; Groundwater

---

1. Introduction

Non-Darcy flows take place at relatively high seepage velocity through porous media such as rockfills, gravel beds and waste dumps. Modelling of such flows is often required in many disciplines including groundwater, geotechnical and environmental engineering. Empirical and theoretical efforts have been made in past decades to extend the Darcy law to the flow through porous media with significant inertial effects. For engineering applications, several formulations of flow resistance have been proposed (Kovács 1981), of which the most typical examples are the quadratic and power models given in the following form:

$$i_s = au_s + bu_s^2 \tag{1}$$

$$i_s = cu_s^m \tag{2}$$

where i_s = hydraulic gradient; u_s = bulk or superficial seepage velocity; a, b and c = coefficients; and m = power varying from 1 to 2. The four parameters (a, b, c and m) can be evaluated from experimental data.

Eq. (1) is also called Forchheimer equation (Bear 1988). It was proposed on the grounds that the seepage-related energy dissipation is taken as a sum of energy losses associated with viscous drag and inertial effects. For the case of creeping flow, the viscous drag is linear and thus the Darcy law prevails, as is represented by the first term on the right-hand-side of Eq. (1). With increasing seepage velocity, deviation from the Darcy law takes place because of flow separation at the lee of particles and/or the onset of turbulence. The deviation, in spite of its origins, finally results in a nonlinear drag, which can be well approximated as a function that is proportional to the squared seepage velocity as given by the second term on the right-hand-side of Eq. (1). Some analytical attempts have been devoted to associate the nonlinear drag with inertial and/or turbulent effects of viscous flow, but the theoretical bases of these attempts are still controversial in the literature (e.g. Bear

1988). Direct numerical simulation appears recently as a practical alternative to visualise the transition of flow from linear to nonlinear behaviour. For example, by solving the Navier-Stokes equations for a two-dimensional disordered porous structure with high porosity, Andrade (1999) demonstrated that the incipient departure from the Darcy law that is in agreement with Eq. (1) can be observed in the laminar regime of fluid flow without including turbulence effects.

In comparison with Eq. (1), the power form [Eq. (2)] also works well, sometimes even better, in representing variations in the pressure drop measured for different seepage velocities (Bordier and Zimmer 2000; Trussell and Chang 1999). Cheng and Chiew (1999) reported that from data-fitting performed for the entire range of the seepage velocity, which was observed through porous column comprising sand or gravel, the estimated power (m) increased with the dimensionless pore length scale.

Although the quadratic law could be somehow derived from the Navier-Stokes equations with certain arguments (Chen et al. 2001), both types of functions are often employed to empirically present data-based correlations. This is because it is still generally unclear that to what content these functions are able to characterize reasonably the physics inherent in the flow phenomena. Other questions worthy of further theoretical efforts include under what conditions the nonlinear term appears, and the viscous drag becomes proportional to the squared seepage velocity. Qualitatively, the above questions about seepage flow may be understood by making an analogy with flow around a spherical object. For the latter case, flow separation behind a particle can occur even prior to the onset of turbulence (van Dyke 1982), which explains the deviation of the settling drag from the linear Stokes regime.

On the other hand, for engineering applications, it would be very interesting to understand how the two laws differ from each other because one form of function may be preferred to the other. Some analyses in this respect have been presented, for example, by

George and Hansen (1992) and Niven (2000). George and Hansen (1992) theoretically showed that the data-based conversions between the two laws are always possible, but the coefficients estimated from one pair to another (i.e. from *a* and *b* to *c* and *m*, or from *c* and *m* to *a* and *b*) is subject to the maximum seepage velocity under consideration. Another conversion study is due to Niven (2000), who first numerically generated a database of the hydraulic gradient with the quadratic function and then fitted to the power function. The results so obtained show that the power law was able to predict the hydraulic gradient within an error of 22%.

In this study, seepage was observed through a laboratory experiment designed with a simplified ordered porous media model. The functional relation of flow resistance is presented on the grounds of dimensional analysis in terms of the friction factor and Reynolds number. The measured results are then fitted to the quadratic and power functions and the variations associated with the parameters included in the functions are examined in detail. In addition, numerical simulations were also conducted to help appreciate relevant micro-flow phenomena localised in the pore domain.

2. Laboratory experiment with ordered porous model

The porous media employed in the experiment were modelled by placing glass beads into a square steel pipe of 3 m in length. The diameter of the glass bead, D, was 16 mm and the cross section of the pipe was measured as $l^2 = 16.4 \times 16.4$ mm^2. The beads were packed closely along the pipe and the bead-to-bead gap was not allowed. However, the movement of beads in the transverse direction was possible because of the small difference (0.4 mm gap) between the bead size and the cross-section dimension, but its effect is considered insignificant. The resulted global porosity was 0.50 and the cross-sectional porosity varied

from 1 to 0.25. Fig. 1 shows a gradual increase in the cross-sectional area of the flow passage (A_p) from the largest blockage (x/D = 0) to the zero blockage (x/D = 0.5), where x is a longitudinal distance measured from the centre of a glass bead. The variation of A_p with x for $0 \le x \le D/2$ is given by

$$\frac{A_p}{l^2} = 1 - \pi\left(\frac{D^2}{4l^2} - \frac{x^2}{l^2}\right) \tag{3}$$

This simplified model is free of irregularities induced by random granular configuration and also facilitates control of flows. In addition, it would be possible to explore details of fluid flowing in the pores with the aid of computational hydrodynamic technique. As shown later in this paper, the results obtained differ quantitatively from those available in the literature for conventional porous media with random configuration. However, they provide an alternative insight into the transition between the linear and non-linear flow domains, and also a well-defined physical model for assessing how well the transition can be described with the quadratic and power functions.

To have a wide range of the Reynolds number, both clear water and water-glycerine mixture were used as the fluid media. The viscosity of the mixture which varied with temperature was measured using a piston-type viscometer manufactured by Cambridge Applied Systems. A few probes applied for different ranges of viscosities were employed. The temperature-dependence of viscosity was first calibrated for a range of temperatures and also fitted empirically using exponential functions. The so-obtained calibration curves were then applied to test cases with individual temperatures taken. The pipe flow was driven using a submergible pump. The error in measuring the pressure drop was less than 2% either using a water-based manometer or mercury-based manometer.

Altogether four series of experiments comprising 242 runs were completed. The test conditions are summarized in Table 1. Four kinds of fluids (G00, G50, G70, and G80) were

prepared by setting the concentration of glycerine roughly at 0%, 50%, 67% and 80%, respectively. The use of the low-molecular weight fluids, glycerine and its aqueous solutions, implies that the experiments done were under the condition of Newtonian fluids. The variations of the hydraulic gradient with the seepage velocity are plotted in Fig. 2. The average flow velocity varied from 0.004 to 0.282 m/s. The use of glycerine-water mixture made available a range of fluid kinematic viscosity (ν) from 0.7 to 35 cSt (10^{-6} m^2/s). As a result, the Reynolds number ($= u_s D/\nu$) varied from 2 to 5550, where u_s is the superficial seepage velocity and D is the bead diameter. The observed flows covered the Darcy-type linear regime and also inertia-dominant nonlinear regime.

3. Dimensional Analysis

Resistance of flows through porous media can be investigated by making an analogy with that considered in conventional pipe flows because both flows are boundary-confined. Several attempts in this respect have been reported in literature (Bear 1988), which involve various geometric simplifications of porous media. These are not replicated in this study. Instead, the consideration presented here only engages two parameters, friction factor and Reynolds number. By drawing an analogy with pipe flows, these two parameters can be redefined by including effects of porous media, so that the flow resistance relationship can be presented in a way similar to the Moody diagram, which is often included in fluid mechanics books.

Here, we use f_p and Re_p to denote the friction factor and Reynolds number for pipe flows, respectively. The relation of f_p-Re_p varies generally with the relative roughness length, but becomes unique for hydrodynamically smooth pipes. In this study, it is assumed that the boundary of interstitial flows is hydrodynamically smooth so that the roughness effect is

ignored. This is acceptable by noting the experimental condition described in the previous section. By definition, f_p is proportional to $(u_{*p}/U_p)^2$ and $Re_p = U_p R_p/\nu$, where $u_{*p} = (gR_p i_p)^{0.5}$, R_p = hydraulic radius, U_p is the average velocity through the pipe, ν = kinematic viscosity of fluid, i_p = hydraulic gradient and g = gravitational acceleration.

In the following, both f_p and Re_p are modified to apply for the case of the interstitial flow in porous media. Being differentiated from the parameters used for pipe flows, those related to seepage flow are denoted with the subscript, s. First, the average velocity U_s is computed with respect to the pore space. If the average porosity is ε, U_s is given by

$$U_s = \frac{u_s}{\varepsilon} \tag{4}$$

where u_s is the bulk or superficial seepage velocity, which is the volumetric flux of fluid per unit area (computed in the spatial domain composed of pores and particle matrix).

Second, the hydraulic radius R_p can be replaced with R_s, the characteristic length of the cross-sectional area of the flow. The latter can be shown to be proportional to the particle size for porous media. For a one-dimensional flow, R_p is defined as the ratio of the cross-sectional area to the wetted perimeter of the flow. This concept can be further extended to the three-dimensional space by defining the hydraulic radius as the ratio of the volume of the interstitial space to the area of the interface between solid and fluid. Consider a porous media of a unit volume. The total volume of the pores within this volume is ε. If the particle diameter is D, the number of the particles enclosed is $(1-\varepsilon)/(\pi D^3/6)$ and the total interfacial area is equal to $\pi D^2(1-\varepsilon)/(\pi D^3/6) = 6(1-\varepsilon)/D$. Then, by ignoring the constant coefficient, the redefined hydraulic radius R_s is proportional to the particle size D, i.e.

$$R_s = \frac{\varepsilon}{1-\varepsilon} D \tag{5}$$

It is noted that the dimensionless pore scale can be defined as $(g/\nu^2)^{1/3} R_s$ (Cheng 2003). With the modified hydraulic radius, the seepage shear velocity can be expressed as

$$u_{*s} = \sqrt{gR_s i_s} = \sqrt{\frac{\varepsilon}{1-\varepsilon} gDi_s} \tag{6}$$

As a result, the flow resistance relation of f_p-Re_p is revised in the form of f_s-Re_s, where f_s is the seepage friction factor defined as

$$f_s = \left(\frac{u_{*s}}{U_s}\right)^2 = \frac{\varepsilon^3}{1-\varepsilon}\frac{gDi_s}{u_s^2} \tag{7}$$

and Re_s is the seepage Reynolds number given by

$$Re_s = \frac{U_s R_s}{\nu} = \frac{1}{1-\varepsilon}\frac{u_s D}{\nu} \tag{8}$$

Approximately, Re_s can be understood as a measure of the ratio of inertial to viscous effect in a 'simplified' pipe flow that represents the porous media.

Since the hydraulic gradient i_s is proportional to the squared shear velocity, u_{*s}^2, the empirical quadratic and power functions, Eqs. (1) and (2), can be re-written respectively in the following dimensionless form:

$$\left(\frac{u_{*s}R_s}{\nu}\right)^2 = A\left(\frac{u_s R_s}{\nu}\right) + B\left(\frac{u_s R_s}{\nu}\right)^2 \quad \text{or} \quad Re_{*s}^2 = ARe_s + BRe_s^2 \tag{9}$$

$$\left(\frac{u_{*s}R_s}{\nu}\right)^2 = C\left(\frac{u_s R_s}{\nu}\right)^M \quad \text{or} \quad Re_{*s}^2 = CRe_s^M \tag{10}$$

where $Re_{*s} = u_{*s}R_s/\nu$ = seepage-related shear Reynolds number; A, B and C = coefficients; and M = exponent. It is noted that in performing the above dimensional transformation, only the characteristic pore scale and kinematic viscosity of fluid are used. It should also be mentioned that the relation given by Eq. (9) actually follows the same form of the Ergun equation (Bear 1988; Cheng 2003),

$$i_s = 150\frac{\nu(1-\varepsilon)^2}{gD^2\varepsilon^3}u_s + 1.75\frac{1-\varepsilon}{gD\varepsilon^3}u_s^2 \tag{11}$$

which suggests that on average, A = 150 and B = 1.75 for natural porous media. These two average values would vary for other artificial porous media, as exemplified later by this study.

4. Comparison of quadratic and power laws

In the subsequent analysis, the experimental data will be used to explore variations in the four parameters, i.e. the three coefficients (A, B and C) and power (M) included in Eqs. (9) and (10) rather than those initially given in Eqs. (1) and (2).

First, we combine all data series in terms of the two dimensionless parameters, Re_{*s} and Re_s. By plotting Re_{*s}^2 against Re_s, it is found the data points collected for the different runs collapsed almost into a single curve, as shown in Fig. 3. Also superimposed in the figure are two asymptotes for very small and large Reynolds numbers. Second, to fit the data to the proposed empirical functions, Eqs. (9) and (10), the combined data series are further sorted according to ascending Re_s-values. As expected, the optimised values for A, B, C and M depend on the range of data selected for the best-fit. To avoid any deviation induced by any subjective data selection, the sorted data series is then divided into eleven subsets and the adjacent two subsets are allowed to overlap by 50%. Next, for each subset of data, the best-fit is then performed and the corresponding values of A, B, C and M are calculated. The results so obtained are plotted in Figs. 4 and 5, where the middle value of the seepage Reynolds number for each subset is used. It is interesting to note that all four parameters are not constant, generally varying with the seepage Reynolds number (Re_s), and in particular, the variations associated with C and M are more appreciable.

Fig. 4 shows that the estimated A-value appears to be a constant at low Reynolds numbers but fluctuates at high Reynolds numbers. The opposite scenario holds for the

estimated *B*-values. Such variations are understandable by noting that the linear term included in the quadratic model is dominant only for small Reynolds numbers and the nonlinear contribution becomes more important for high Reynolds numbers. On the other hand, the variations in A and B, which are not small, imply that the quadratic law could not represent exactly the characteristics of porous media flows. This observation is not consistent with theoretical attempts that favour the quadratic law.

The result presented in Fig. 5, despite the scattering data points, clearly demonstrates that both *C* and *M* vary to a great extent with the Reynolds number. This is somehow not consistent with the assumption made implicitly in performing data-fit with the power model. The significant variation of *C* (or *M*) with the Reynolds number means that a single value of *C* (or *M*) is not attainable in principle for seepage flow with varying velocities for a given porous medium.

A further inspection of Fig. 5 indicates that with increasing Reynolds number or inertial effect, the *C*-value reduces from *A* to *B* (i.e. $B \le C \le A$) while the *M*-value increases from 1 to 2 (i.e. $1 \le M \le 2$). This suggests that a possible correlation would exist among the four parameters, for example, between the two ratios, $(A-C)/(C-B)$ and $(2-M)/(M-1)$, as shown in Fig. 6.

From the above data-fit exercise, it is observed that the quadratic model is generally applicable in spite of the variations in the two coefficients. In contrast, the power model may approximate well the measurements of the pressure drop provided only that the range of seepage velocity under consideration is not large. This is because both the coefficient and power included in the power model are very sensitive to the seepage Reynolds number.

If the prediction by the quadratic model is assumed to be exact, the two parameters, *C* and *M*, can be theoretically interrelated. This can be shown by considering the following two equations, which are the simplified versions of Eqs. (9) and (10) used for data-fitting,

$$y_1 = Ax + Bx^2 \tag{12}$$

$$y_2 = Cx^M \tag{13}$$

To determine the relationship among the coefficients (A, B and C) and power (M), we first assume that $y_1 \approx y_2$ for any x, which yields

$$A + Bx = Cx^{M-1} \tag{14}$$

Then, let $dy_1/dx \approx dy_2/dx$, one gets

$$A + 2Bx = CMx^{M-1} \tag{15}$$

Solving Eqs. (14) and (15) for x,

$$x = \frac{A}{B}\frac{M-1}{2-M} \tag{16}$$

Substituting Eq. (16) into Eq. (14) gives

$$C = \frac{B}{M-1}\left(\frac{A}{B}\frac{M-1}{2-M}\right)^{2-M} \tag{17}$$

From Eq. (17), it follows that as expected, C varies between A and B, approaching A as $M \to 1$ and B as $M \to 2$. Using Eq. (17), C can be estimated directly for M varying within a limited range for a given dataset, and vice versa. The results computed with Eq. (17) are plotted in Fig. 7, showing that it gives a good representation of the relation among the estimated parameters. Here the values of A and B are taken as 976 and 1.0, respectively, which are obtained by fitting Eq. (9) to the entire dataset.

5. Discussions

Various artificial porous media models have been used in previous studies, many being designed for numerical simulations and only a few for laboratory investigations. In light of the studies summarised by Hlushkou and Tallarek (2006), the seepage flow investigated in

this study would remain to be Darcian for $Re_s < 5.4$ (inertial contribution$\approx$ 5%), laminar for $Re_s < 240$ (inertial contribution$\approx$70%); and turn to be turbulent for $Re_s > 1200$ (inertial contribution$\approx$90%). These critical values are generally in good agreement with the results shown in Fig. 3.

In addition to the two empirical laws, a cubic law (see Fourar et al. 2004) has been also applied for describing the onset of the non-linear behaviour. With the data collected in this study, best-fit exercises show that the cubic law predicts the measurements with large deviations. For example, the average errors are 26.1%, 11.4%, 5.4% and 3.3% for Cases G00, G50, G70 and G80, respectively. In comparison, the quadratic function yields lower errors, which are 1.1%, 4.0%, 1.9% and 2.9%, respectively, for the four cases.

To further understand the non-linear effect, numerical simulations (11 runs in total) were also performed to visualise micro-flow phenomena confined in the pore space. The Navier-Stokes equations were solved using ANSYS® CFX® translational periodicity interface technique with approximately 2×10^6 control volumes (nodes). The simulations converged well for the RMS-residuals less than 10^{-5} and the maximum residuals less than 0.001. The error between the measured and simulated seepage velocity was less than 16%, which is acceptable for similar CFD studies by considering the inherent uncertainties associated with the numerical simulations and laboratory measurements.

To highlight typical flow phenomenon, a vertical plane parallel to the side wall of the tube is selected at z = 6 mm, as shown in Fig. 8(a). The plane passes almost through the flow zone with high velocity. For comparison, the velocity contour is also plotted in Fig. 8(a) on the cross section at x = 0 for $Re_s = 2.0$. The associated streamlines are shown in Figs. 8(b) to 8(d) for Re_s increasing from 4.2 to 880. It can be observed that with increasing inertial effects, the recirculation zone increases gradually in size, which implies that the seepage flow transition occurs from creeping to inertia-dominated regime. Furthermore, the

recirculation zones are characterized largely by low velocity and constant pressure distribution, which is as shown in Figs. 9(a) and 9(b) for Re_s = 880. Fig. 9(b) also demonstrates that high-shear appears through the narrow channels. It is believed that both high-shear flows and recirculation zones are dissipative in nature and thus closely associated with the development of the non-linear effects, even before the onset of turbulence.

6. Conclusions

Both quadratic and power laws, which are often used as extensions of the Darcy law for inertia-affected flows through porous media, are reformulated in this paper in terms of seepage Reynolds numbers. The parameters included in the two laws are then estimated from experimental data that were collected for a simplified porous model of ordered glass beads. The results show that the two coefficients associated with the quadratic law vary differently; the coefficient used for the linear term fluctuates for large Reynolds number and that for nonlinear term varies significantly for low Reynolds number. On the other hand, the two parameters (i.e., the coefficient and power) included in the power law vary more significantly and also correlate to each other. The relation among the four parameters that is analytically derived is in good agreement with that estimated from experimental data. This study suggests that the quadratic law generally represents well (but not exactly) the resistance of the seepage flow including the Darcy and non-Darcy regimes, while the power law is applicable only when the seepage velocity varies within a limited range. CFD simulation study was also conducted to aid visualization of the flow phenomenon in the porous medium. The simulation results show that the fluid transport in the porous model is subject to the dissipative high-shear and pressure losses, which may explain the highly nonlinear behaviour.

Acknowledgements

The writer gratefully acknowledges the efforts made by H. P. Liew, S. T. Soh, and M. M. Ng for collecting the experimental data. Thanks also go to K. H. Chia and K. H. Lim for their assistance in the experiment construction and instrument setup.

References

Andrade, J. S., Costa, U. M. S., Almeida, M. P., Makse, H. A., and Stanley, H. E. (1999). "Inertial effects on fluid flow through disordered porous media." *Physical Review Letters*, 82(26), 5249-5252.

Bear, J. (1988). *Dynamics of fluids in porous media*, Dover, New York.

Bordier, C., and Zimmer, D. (2000). "Drainage equations and non-Darcian modelling in coarse porous media or geosynthetic materials." *Journal of Hydrology*, 228(3-4), 174-187.

Chen, Z. X., Lyons, S. L., and Qin, G. (2001). "Derivation of the Forchheimer law via homogenization." *Transport in Porous Media*, 44(2), 325-335.

Cheng, N. S. (2003). "Application of Ergun equation to computation of critical shear velocity subject to seepage." *Journal of Irrigation and Drainage Engineering-ASCE*, 129(4), 278-283.

Cheng, N. S., and Chiew, Y. M. (1999). "Incipient sediment motion with upward seepage." *Journal of Hydraulic Research*, 37(5), 665-681.

Fourar, M., Radilla, G., Lenormand, R., and Moyne, C. (2004). "On the non-linear behavior of a laminar single-phase flow through two and three-dimensional porous media." *Advances in Water Resources*, 27(6), 669-677.

George, G. H., and Hansen, D. (1992). "Conversion between Quadratic and Power Law for Non-Darcy Flow." *Journal of Hydraulic Engineering-ASCE*, 118(5), 792-797.

Hlushkou, D., and Tallarek, U. (2006). "Transition from creeping via viscous-inertial to turbulent flow in fixed beds." *Journal of Chromatography A*, 1126(1-2), 70-85.

Kovács, G. (1981). *Seepage hydraulics*, Elsevier Scientific Pub. Co., Amsterdam ; New York.

Niven, R. K. (2000). "Incipient sediment motion with upward seepage - Discussion." *Journal of Hydraulic Research*, 38(6), 475-477.

Trussell, R. R., and Chang, M. (1999). "Review of flow through porous media as applied to head loss in water filters." *Journal of Environmental Engineering-ASCE*, 125(11), 998-1006.

van Dyke, M. (1982). *An album of fluid motion*, Parabolic Press, Stanford, Calif.

Table 1. Experimental data collected for the four series.

Series G00											
Run	**u_s (m/s)**	**i**	**ν(m^2/s)**	**Run**	**u_s (m/s)**	**i**	**ν(m^2/s)**	**Run**	**u_s (m/s)**	**i**	**ν(m^2/s)**
1	0.2817	1.898	8.1E-07	28	0.1784	0.794	8.0E-07	55	0.0883	0.215	8.3E-07
2	0.2777	1.840	8.1E-07	29	0.1721	0.752	8.0E-07	56	0.0864	0.207	8.3E-07
3	0.2754	1.814	8.1E-07	30	0.1666	0.710	8.0E-07	57	0.0855	0.201	8.3E-07
4	0.2736	1.793	8.1E-07	31	0.1607	0.664	8.0E-07	58	0.0829	0.194	8.2E-07
5	0.2704	1.760	7.9E-07	32	0.1566	0.622	8.0E-07	59	0.0803	0.181	8.2E-07
6	0.2663	1.714	7.9E-07	33	0.1547	0.605	7.8E-07	60	0.0779	0.171	8.2E-07
7	0.2629	1.672	7.9E-07	34	0.1504	0.580	7.9E-07	61	0.0743	0.158	8.2E-07
8	0.2600	1.630	7.9E-07	35	0.1464	0.546	7.9E-07	62	0.0704	0.144	8.2E-07
9	0.2547	1.588	7.9E-07	36	0.1440	0.521	7.8E-07	63	0.0668	0.130	8.1E-07
10	0.2507	1.529	7.9E-07	37	0.1402	0.512	7.9E-07	64	0.0640	0.123	8.1E-07
11	0.2474	1.470	7.9E-07	38	0.1359	0.483	7.9E-07	65	0.0613	0.114	8.1E-07
12	0.2422	1.420	7.9E-07	39	0.1319	0.454	7.9E-07	66	0.0577	0.102	8.1E-07
13	0.2410	1.399	8.1E-07	40	0.1256	0.420	7.9E-07	67	0.0546	0.095	8.1E-07
14	0.2389	1.378	8.3E-07	41	0.1188	0.378	7.9E-07	68	0.0518	0.086	8.1E-07
15	0.2347	1.327	8.3E-07	42	0.1117	0.340	7.9E-07	69	0.0484	0.076	8.0E-07
16	0.2299	1.285	8.2E-07	43	0.1072	0.311	7.8E-07	70	0.0454	0.071	8.0E-07
17	0.2263	1.243	8.2E-07	44	0.0992	0.269	7.8E-07	71	0.0426	0.062	7.9E-07
18	0.2217	1.193	8.2E-07	45	0.0934	0.244	7.8E-07	72	0.0384	0.052	7.9E-07
19	0.2163	1.151	8.2E-07	46	0.0857	0.206	7.8E-07	73	0.0352	0.044	7.9E-07
20	0.2114	1.105	8.1E-07	47	0.1050	0.298	8.5E-07	74	0.0328	0.040	7.9E-07
21	0.2083	1.079	8.1E-07	48	0.1037	0.289	8.5E-07	75	0.0305	0.036	7.9E-07
22	0.2054	1.046	8.1E-07	49	0.1011	0.279	8.5E-07	76	0.0250	0.027	7.9E-07
23	0.2029	1.012	8.1E-07	50	0.0990	0.268	8.4E-07	77	0.0214	0.022	7.8E-07
24	0.1962	0.966	8.1E-07	51	0.0956	0.252	8.4E-07	78	0.0160	0.014	7.8E-07
25	0.1919	0.928	8.1E-07	52	0.0941	0.243	8.4E-07	79	0.0130	0.011	7.8E-07
26	0.1882	0.878	8.1E-07	53	0.0922	0.235	8.4E-07	80	0.0124	0.010	7.7E-07
27	0.1839	0.836	8.0E-07	54	0.0903	0.227	8.3E-07				
Series G50											
81	0.2245	1.936	4.4E-06	101	0.1642	1.071	4.3E-06	121	0.0653	0.252	4.2E-06
82	0.2222	1.915	4.4E-06	102	0.1568	1.021	4.3E-06	122	0.0602	0.218	4.2E-06
83	0.2209	1.898	4.4E-06	103	0.1532	0.974	4.3E-06	123	0.0550	0.202	4.2E-06
84	0.2177	1.861	4.4E-06	104	0.1478	0.932	4.3E-06	124	0.0508	0.176	4.2E-06
85	0.2173	1.819	4.4E-06	105	0.1417	0.895	4.3E-06	125	0.0464	0.164	4.2E-06
86	0.2157	1.772	4.4E-06	106	0.1389	0.861	4.3E-06	126	0.0424	0.147	4.4E-06
87	0.2108	1.726	4.4E-06	107	0.1373	0.823	4.3E-06	127	0.0446	0.143	4.2E-06
88	0.2098	1.680	4.4E-06	108	0.1331	0.773	4.3E-06	128	0.0399	0.126	4.2E-06
89	0.2042	1.646	4.4E-06	109	0.1273	0.722	4.3E-06	129	0.0363	0.130	4.4E-06
90	0.2027	1.600	4.4E-06	110	0.1197	0.689	4.3E-06	130	0.0337	0.105	4.2E-06
91	0.1967	1.541	4.4E-06	111	0.1152	0.638	4.3E-06	131	0.0285	0.088	4.2E-06
92	0.1910	1.466	4.4E-06	112	0.1091	0.596	4.3E-06	132	0.0249	0.071	4.2E-06
93	0.1874	1.428	4.3E-06	113	0.1031	0.512	4.2E-06	133	0.0325	0.105	4.3E-06

94	0.1859	1.386	4.3E-06	114	0.1008	0.491	4.2E-06	134	0.0283	0.092	4.3E-06
95	0.1850	1.357	4.3E-06	115	0.0940	0.458	4.2E-06	135	0.0212	0.067	4.3E-06
96	0.1841	1.319	4.3E-06	116	0.0922	0.424	4.2E-06	136	0.0166	0.050	4.3E-06
97	0.1812	1.294	4.3E-06	117	0.0874	0.391	4.2E-06	137	0.0157	0.046	4.3E-06
98	0.1777	1.243	4.3E-06	118	0.0817	0.365	4.2E-06	138	0.0115	0.034	4.3E-06
99	0.1721	1.184	4.3E-06	119	0.0771	0.328	4.2E-06	139	0.0094	0.025	4.3E-06
100	0.1678	1.126	4.3E-06	120	0.0698	0.286	4.2E-06				
Series G70											
140	0.1503	1.945	1.3E-05	157	0.1079	1.159	1.2E-05	174	0.0629	0.559	1.1E-05
141	0.1484	1.898	1.3E-05	158	0.1054	1.134	1.2E-05	175	0.0587	0.525	1.1E-05
142	0.1451	1.844	1.3E-05	159	0.1033	1.084	1.2E-05	176	0.0544	0.462	1.1E-05
143	0.1428	1.798	1.3E-05	160	0.1019	1.054	1.2E-05	177	0.0490	0.420	1.1E-05
144	0.1408	1.760	1.3E-05	161	0.0981	1.008	1.2E-05	178	0.0441	0.365	1.1E-05
145	0.1380	1.676	1.2E-05	162	0.0947	0.962	1.2E-05	179	0.0410	0.323	1.1E-05
146	0.1340	1.630	1.2E-05	163	0.0922	0.924	1.2E-05	180	0.0351	0.269	1.1E-05
147	0.1319	1.592	1.2E-05	164	0.0895	0.903	1.2E-05	181	0.0306	0.235	1.1E-05
148	0.1299	1.537	1.2E-05	165	0.0872	0.848	1.2E-05	182	0.0269	0.197	1.1E-05
149	0.1295	1.512	1.2E-05	166	0.0838	0.819	1.2E-05	183	0.0227	0.160	1.1E-05
150	0.1279	1.483	1.2E-05	167	0.0835	0.790	1.2E-05	184	0.0186	0.134	1.1E-05
151	0.1251	1.445	1.2E-05	168	0.0810	0.769	1.1E-05	185	0.0162	0.105	1.1E-05
152	0.1223	1.403	1.2E-05	169	0.0786	0.748	1.1E-05	186	0.0122	0.076	1.1E-05
153	0.1205	1.352	1.2E-05	170	0.0772	0.710	1.1E-05	187	0.0092	0.055	1.1E-05
154	0.1163	1.306	1.2E-05	171	0.0754	0.693	1.1E-05	188	0.0065	0.038	1.1E-05
155	0.1151	1.256	1.2E-05	172	0.0700	0.647	1.1E-05	189	0.0042	0.025	1.1E-05
156	0.1108	1.210	1.2E-05	173	0.0672	0.613	1.1E-05				
Series G80											
190	0.0733	1.886	3.7E-05	208	0.0443	1.025	3.9E-05	226	0.0218	0.458	3.7E-05
191	0.0715	1.852	3.7E-05	209	0.0434	0.970	3.7E-05	227	0.0214	0.454	3.8E-05
192	0.0697	1.806	3.8E-05	210	0.0411	0.958	3.9E-05	228	0.0213	0.433	3.5E-05
193	0.0692	1.768	3.8E-05	211	0.0407	0.937	3.8E-05	229	0.0187	0.391	3.6E-05
194	0.0683	1.726	3.7E-05	212	0.0415	0.903	3.7E-05	230	0.0194	0.382	3.5E-05
195	0.0669	1.693	3.7E-05	213	0.0381	0.853	3.8E-05	231	0.0172	0.344	3.6E-05
196	0.0648	1.659	4.0E-05	214	0.0376	0.802	3.5E-05	232	0.0162	0.315	3.6E-05
197	0.0637	1.575	3.7E-05	215	0.0349	0.798	3.7E-05	233	0.0146	0.294	3.6E-05
198	0.0603	1.516	4.0E-05	216	0.0342	0.764	3.8E-05	234	0.0137	0.256	3.6E-05
199	0.0600	1.470	4.0E-05	217	0.0349	0.735	3.5E-05	235	0.0123	0.235	3.7E-05
200	0.0574	1.436	4.1E-05	218	0.0319	0.693	3.8E-05	236	0.0109	0.223	3.5E-05
201	0.0552	1.357	4.0E-05	219	0.0315	0.643	3.5E-05	237	0.0083	0.181	4.0E-05
202	0.0538	1.289	3.9E-05	220	0.0301	0.617	3.5E-05	238	0.0088	0.155	3.6E-05
203	0.0529	1.247	3.9E-05	221	0.0290	0.584	3.5E-05	239	0.0063	0.130	3.6E-05
204	0.0525	1.218	3.8E-05	222	0.0279	0.584	3.8E-05	240	0.0061	0.109	3.6E-05
205	0.0508	1.214	3.7E-05	223	0.0249	0.504	3.7E-05	241	0.0049	0.105	3.9E-05
206	0.0480	1.105	3.7E-05	224	0.0232	0.487	3.7E-05	242	0.0043	0.076	3.5E-05
207	0.0456	1.037	3.7E-05	225	0.0226	0.470	3.5E-05				

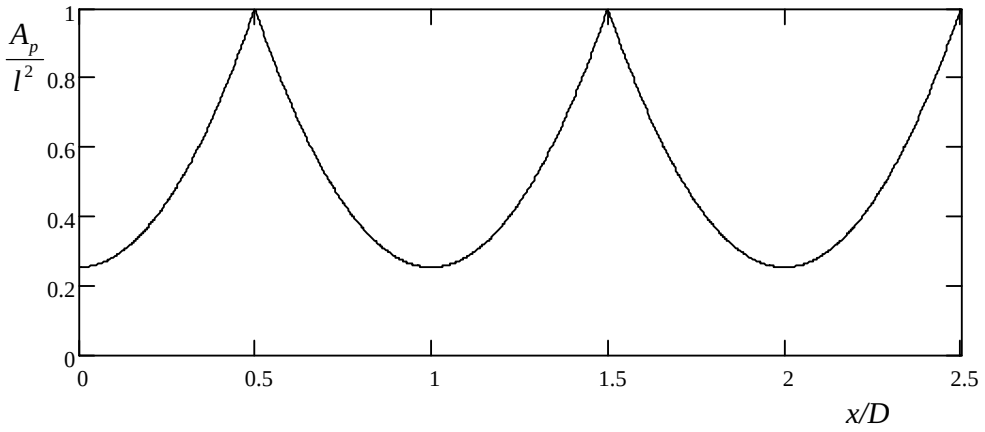

Fig. 1. Variation of cross-sectional area of flow passage.

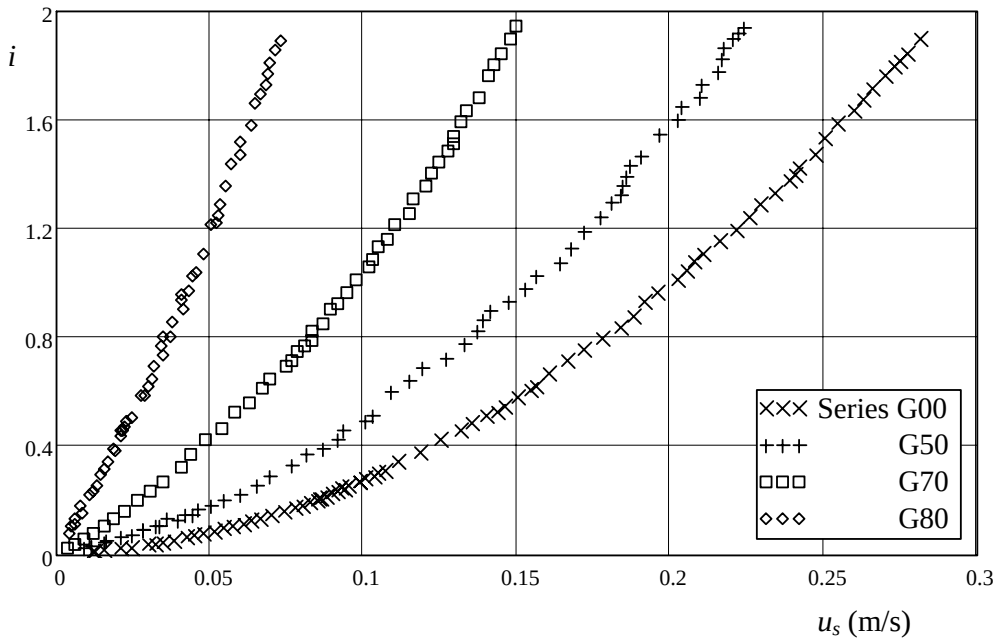

Fig. 2. Observations of hydraulic gradient varying with superficial seepage velocity.

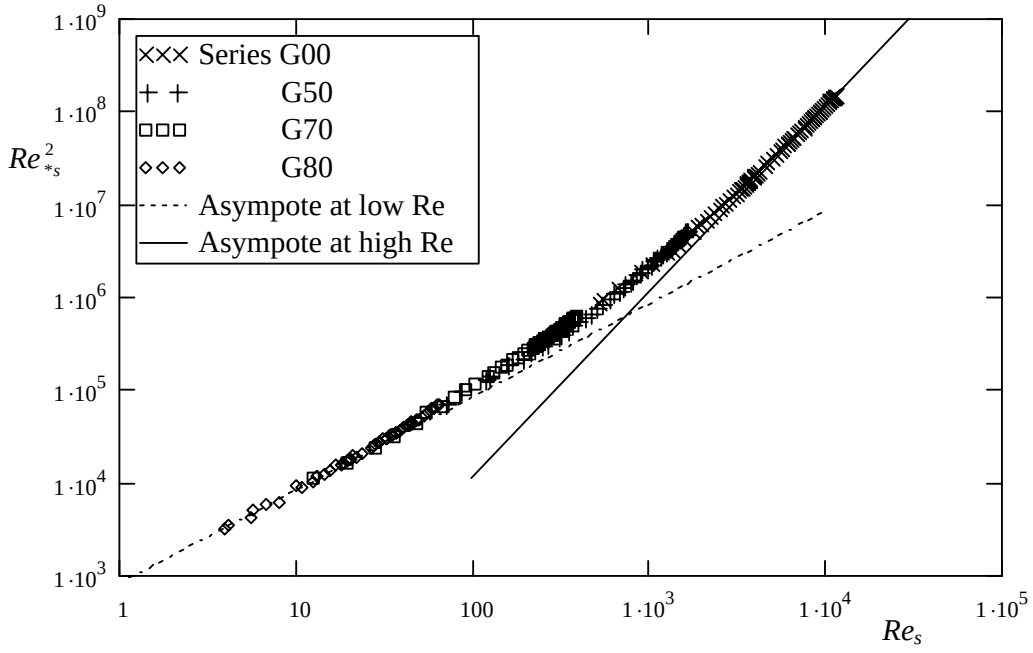

Fig. 3. Experimental data presented in dimensionless parameters, Re^2_{*s} and Re_s. Asymptotes are superimposed for very small and large Reynolds numbers.

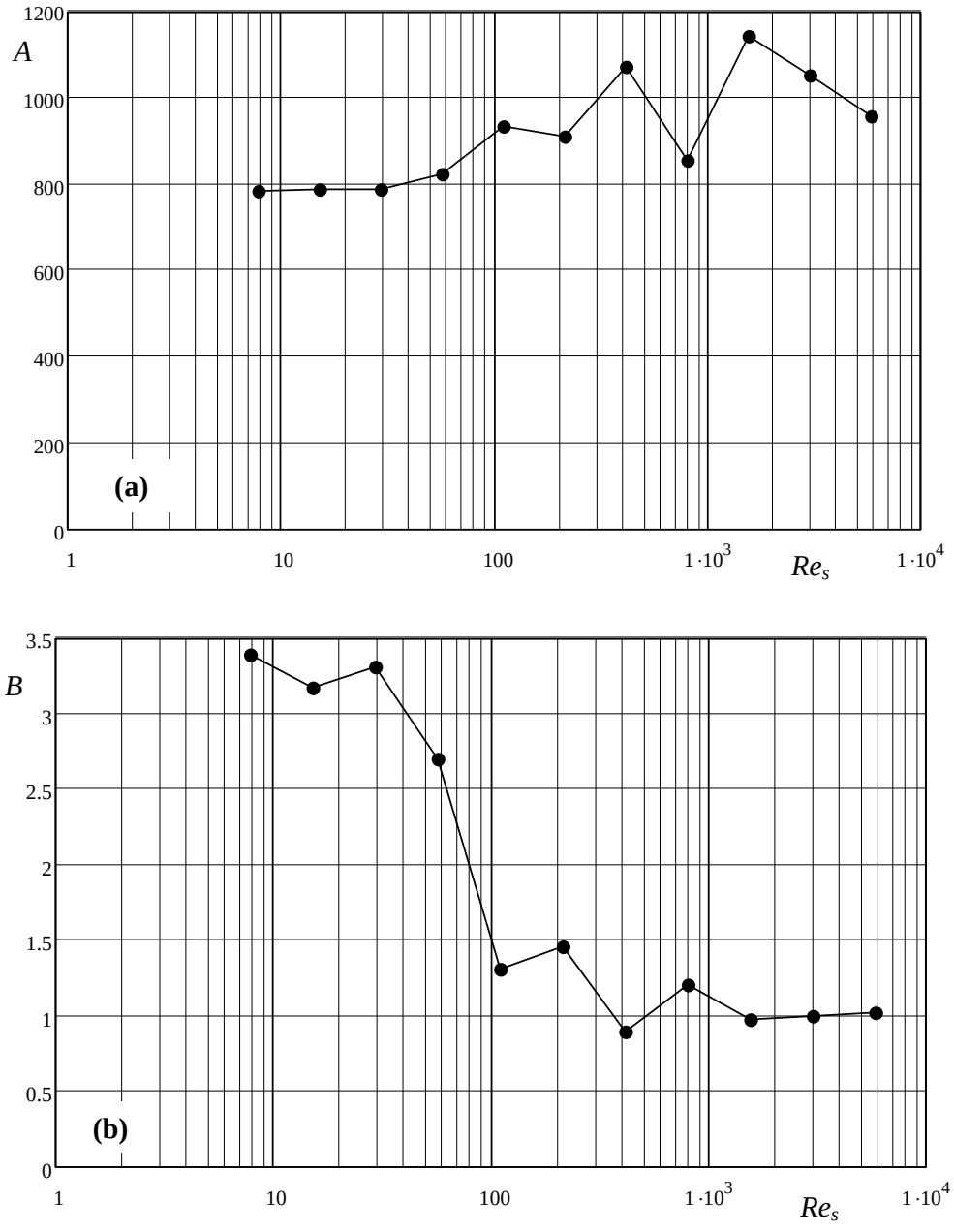

Fig. 4. Variations of the coefficients, *A* and *B*, included in the quadratic law.

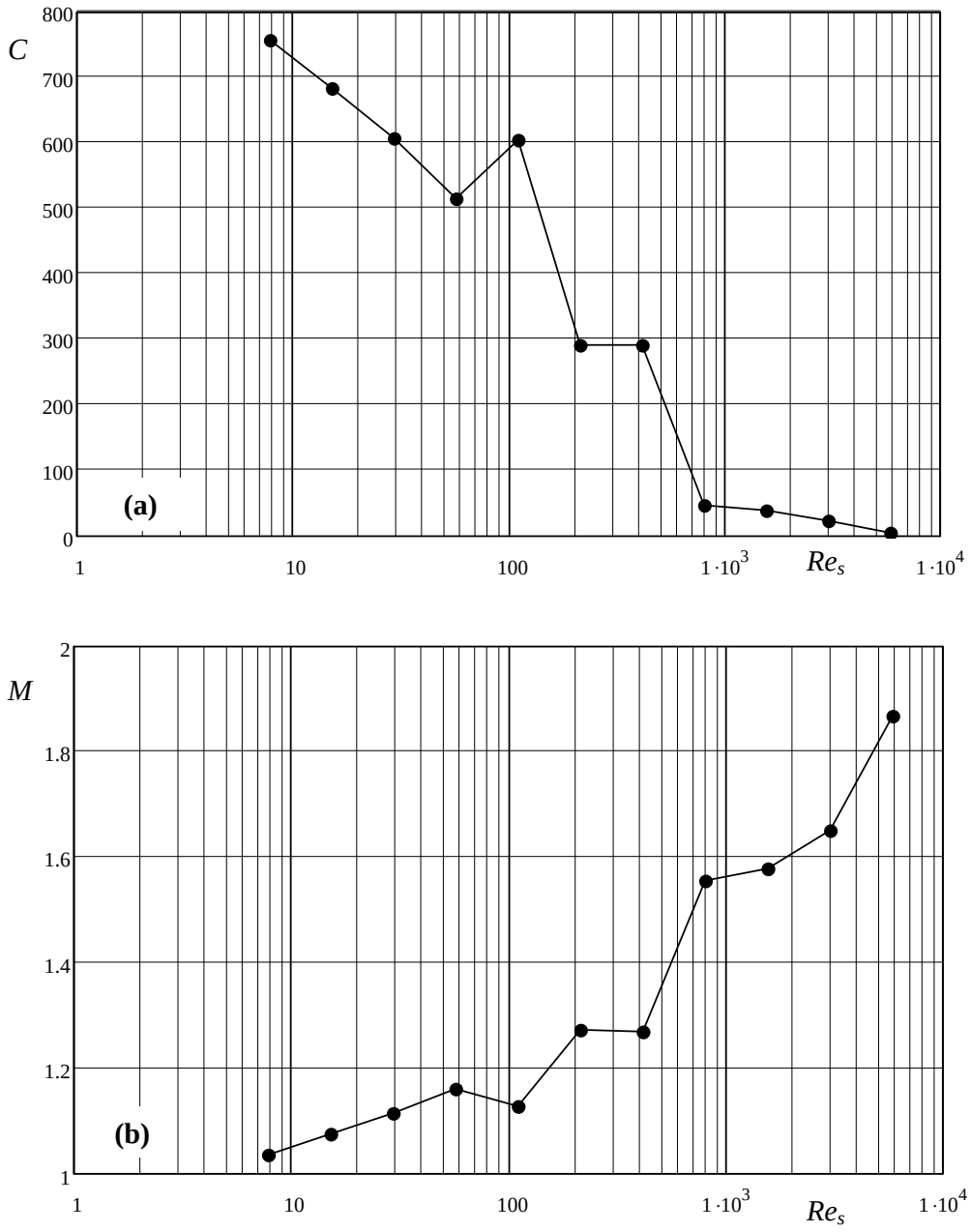

Fig. 5. Variations of the parameters, *C* and *M*, included in the power law.

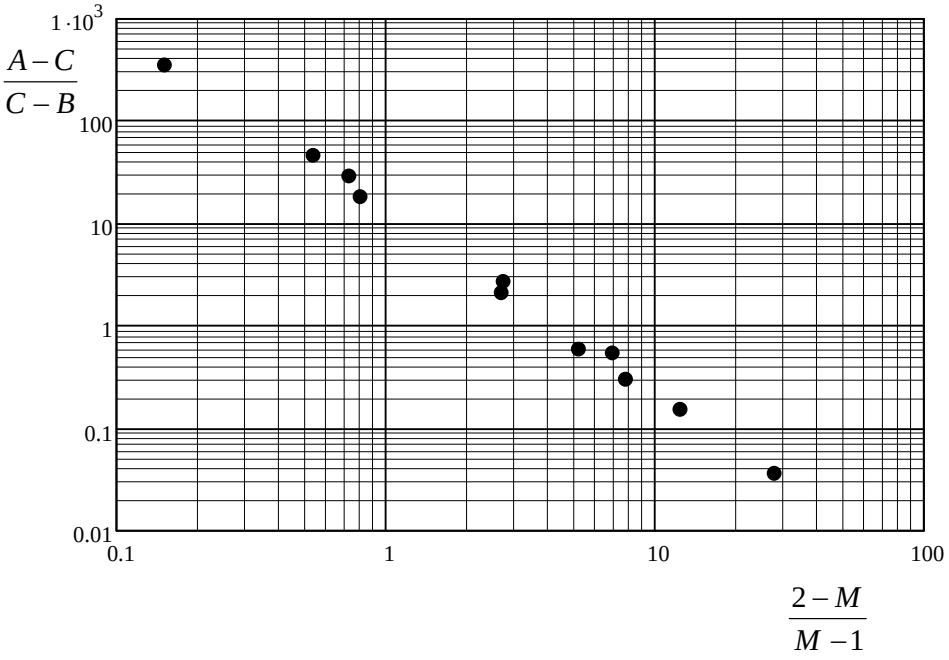

Fig. 6. Relation between (A-C)/(C-B) and (2-M)/(M-1).

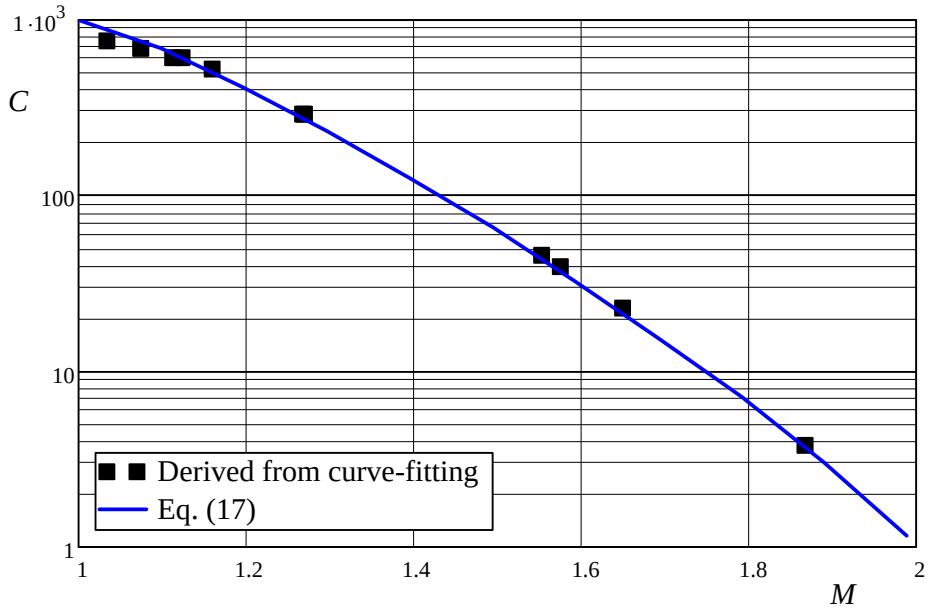

Fig. 7. Comparison of the C-values computed with Eq. (17) and those derived from best-fit of experimental data.

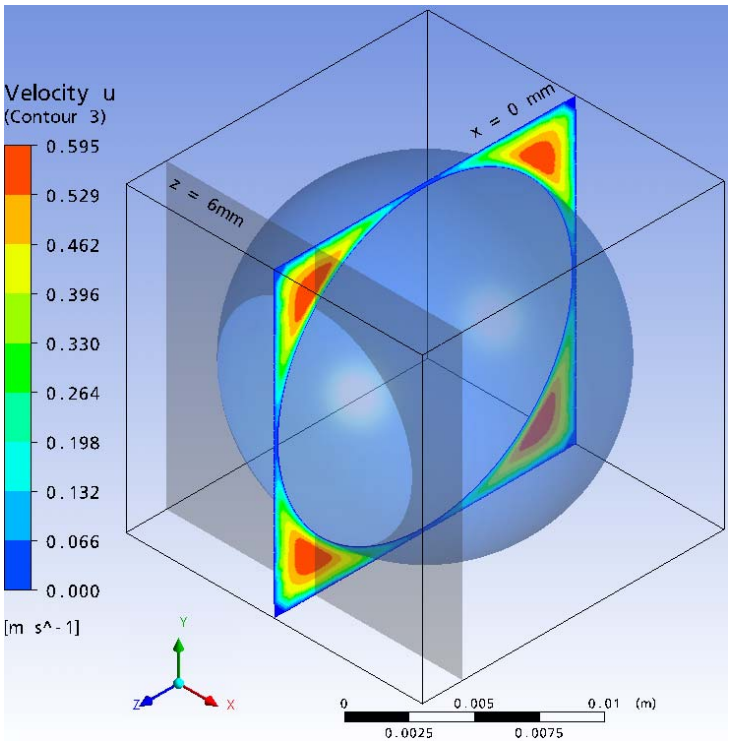

(a) Vertical plane selected at z = 6 mm

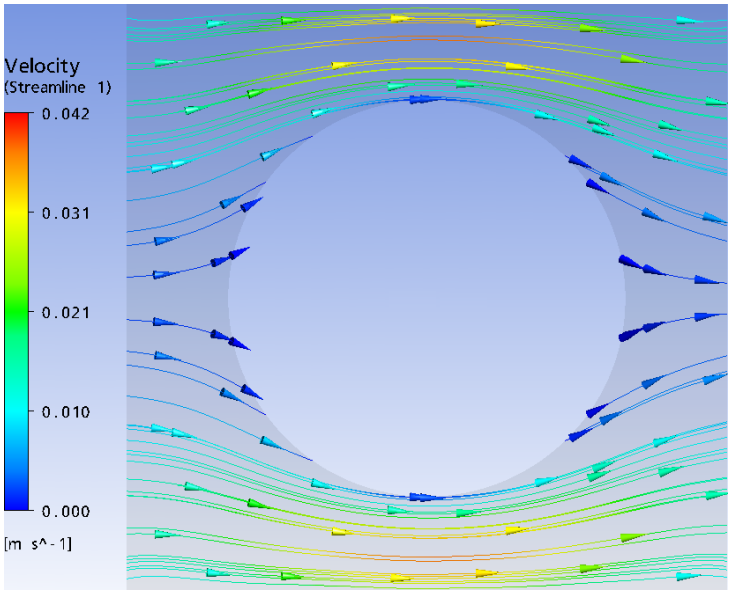

(b) Re_s = 4.2

Fig. 8. Streamlines computed for the longitudinal vertical plane at z = 6 mm.

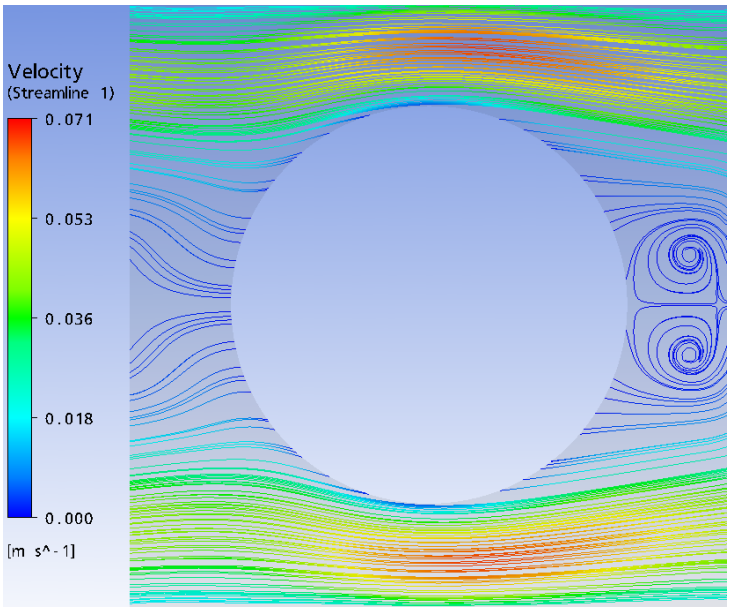

(c) $Re_s = 41.6$

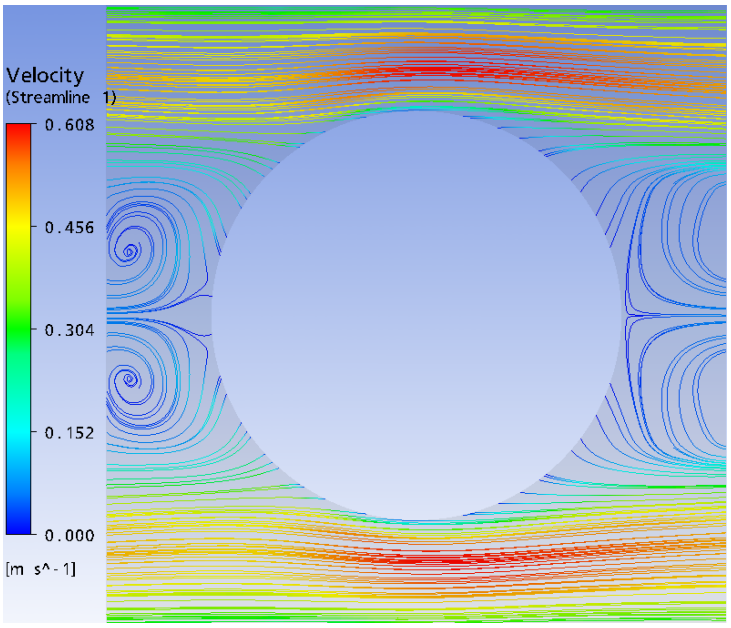

(d) $Re_s = 880$

Fig. 8. Streamlines computed for the longitudinal vertical plane at z = 6 mm.

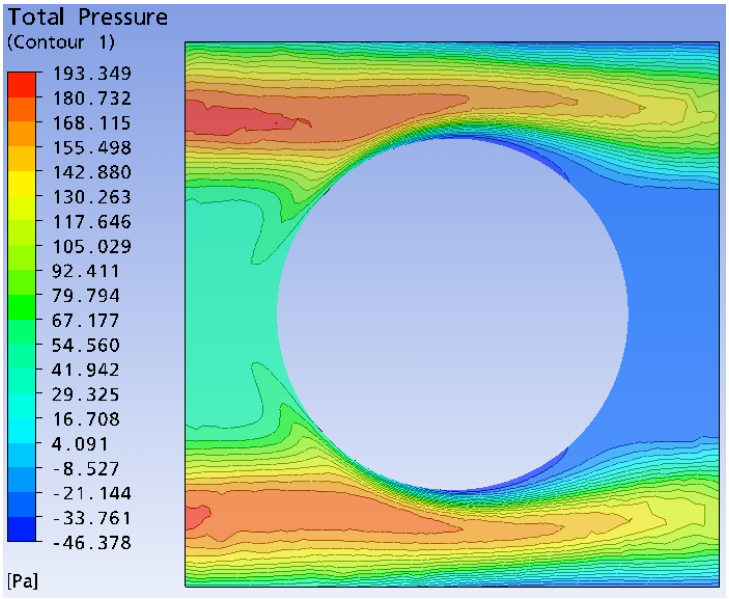

(a) Pressure contour

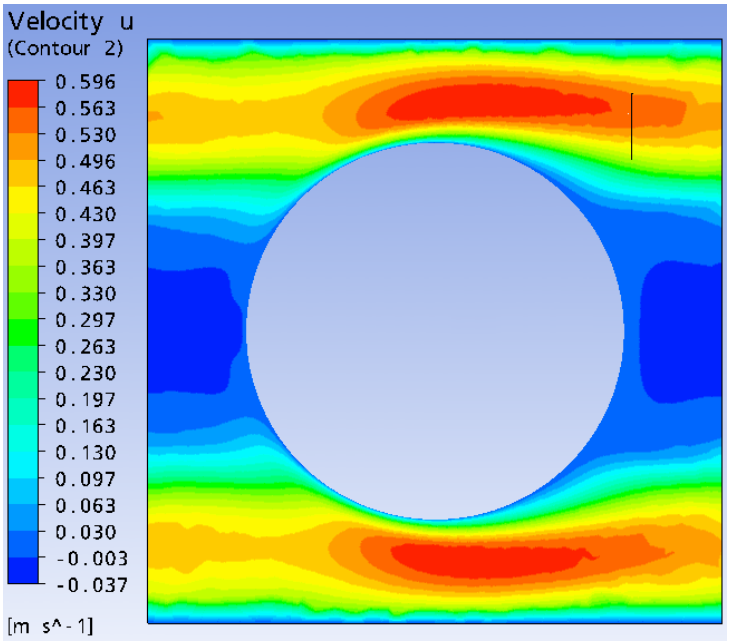

(b) Velocity contour (u)

Fig. 9. Pressure and longitudinal-velocity distributions at Re_s = 880.